

Molecular multiresolution surfaces

G. W. Wei^{1,2,*}, Yuhui Sun¹, Y. C. Zhou¹ and M. Feig³

¹Department of Mathematics

Michigan State University, MI 48824, USA

²Department of Electrical and Computer Engineering

Michigan State University, MI 48824, USA

³Department of Biochemistry and Molecular Biology

Michigan State University, MI 48824, USA

September 18, 2018

Abstract

The surface of a molecule determines much of its chemical and physical property, and is of great interest and importance. In this Letter, we introduce the concept of molecular multiresolution surfaces as a new paradigm of multiscale biological modeling. Molecular multiresolution surfaces contain not only a family of molecular surfaces, corresponding to different probe radii, but also the solvent accessible surface and van der Waals surface as limiting cases. All the proposed surfaces are generated by a novel approach, the diffusion map of continuum solvent over the van der Waals surface of a molecule. A new local spectral evolution kernel is introduced for the numerical integration of the diffusion equation in a single time step.

Molecular surface [23] is one of the most important concepts in modern biochemistry and molecular biology. Albeit molecular surfaces are merely a conventional imitation of molecular boundaries, it has been shown that such models can often explain fundamental physical and chemical effects. For example, the stability and solubility of macromolecules, such as protein, DNA and RNA, are determined by how their surfaces interact with solvent and/or other surrounding molecules. Therefore, the structure and function of macromolecules depend on the features of their molecular surfaces. Important applications of molecular surfaces [23], as well as solvent accessible surfaces [17] and van der Waals surfaces, are flaring in protein folding [20, 28], protein-protein interfaces [7], oral drug classification [2], DNA binding and bending [9], parameterization of heat capacity changes [20], macromolecular docking [16], enzyme catalysis [19], calculation of solvation energies [22], molecular dynamics [8], and implicit solvent models [1, 11, 26].

*Corresponding author.

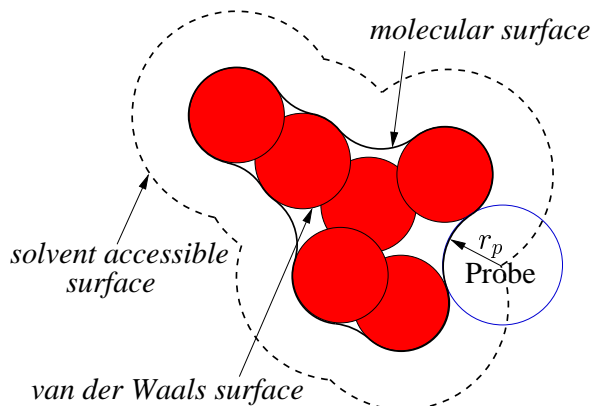


Figure 1: Illustration of various surfaces.

Molecular surface [23], also called solvent excluded surface, is the surface that encloses the solvent excluded volume [5], and can be defined as a smooth envelope traced out by the surface of a probe sphere rolled over the molecular van der Waals surface. The latter is a collection of all the unburied atomic surfaces of the molecule, see Fig. 1. The estimation and analysis of solvent accessible surfaces and molecular surfaces have attracted much attention in the past three decades after the first calculation of molecular surfaces by Greer and Bush [15]. A variety of methods have been proposed, including the Gauss-Bonnet theorem [5, 24], closed-form analytical method [13], space transformation [12], alpha shape theory [18], triangulation [6, 34], Cartesian grid based methods [26], contour-buildup algorithm [29], binary tree [27], and parallel methods [30]. Despite of much success, in general, calculation of molecular surfaces is both topologically and computationally challenging due to the multiple overlap of atomic spheres, overall irregular structure of a macromolecule, and self-intersecting singularities [14, 27]. The situation where the probe sphere is simultaneously tangent to four atoms poses another challenge [10]. Molecular surface calculations are the bottleneck in the molecular dynamics of macromolecules, where the molecular surfaces are computed billions of times in the course of the simulation.

About four decades ago, Benoit Mandelbrot posed the profound question of how one measures the length of a coastline in his paper entitled “How long is the coastline of Great Britain- Statistical self-similarity and fractional dimension” [21]. The answer depends on what scale the measurement is being made — one arrives at a different length by using a different scale. It is easy to envision that the molecular surface of a molecule depends the scale of the probe. As biological phenomena occur over a wide range of length scales, molecular multiresolution surfaces ought to provide the scientific community with a multiscale framework to reveal complex biological processes across scales. Unfortunately, such a multiscale framework does not yet exist.

The objective of the present work is to introduce the concept of molecular mul-

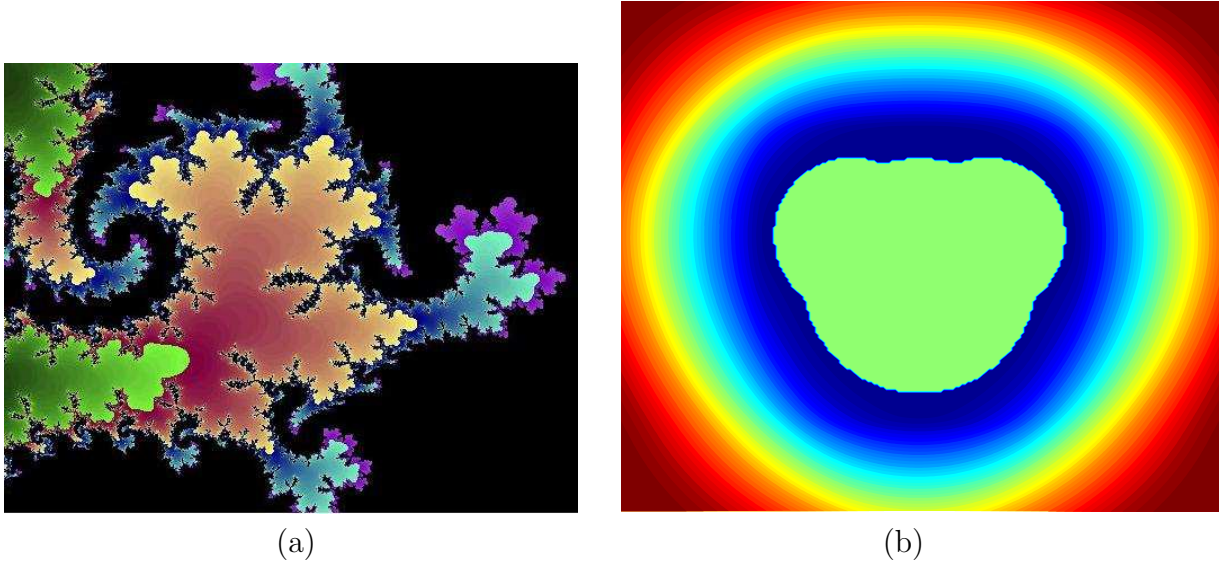


Figure 2: Multiscale surfaces marked up by flow contours. (a) The diffusion map of a fractal (Courtesy: The Mandelbrot Explorer Gallery); (b) The multiresolution surfaces of a water molecule.

multiresolution surfaces both as a multiscale framework for biological modeling and as a unified description of the van der Waals surface, solvent accessible surface and molecular surface. The essential idea is similar to the multiresolution profiles of a fractal, generated by restricted diffusion, see Fig. 2. Use is made to continuum solvent and its curvature-controlled diffusion. The mathematical description of the solvent diffusion process is formulated by appropriate reaction-diffusion equations. All geometric features of a molecular surface, such as convex spherical patches, saddle-shaped pieces of tori, and concave reentrant faces, are naturally accounted by the geometric property of partial differential equations with appropriate initial-boundary conditions. A family of molecular multiresolution surfaces are found to correspond to different probe radii, and are generated in the continuous distribution of solvent density. The van der Waals surface is a special case in which the probe radius vanishes. A fast computational algorithm is introduced to generate molecular multiresolution surfaces in a single step of time evolution.

Without the loss of generality, we assume that the fluid flow of continuum solvent has a density distribution $\rho(\mathbf{r}, t)$ at a space-time location (\mathbf{r}, t) , where $\mathbf{r} \in \mathbb{R}^3$ and $t \in [0, \infty)$. For an arbitrarily small volume Ω , the motion of the solvent density is characterized by density flux $\mathbf{J}(\mathbf{r}, t)$ through the surface of the volume, $\partial\Omega$. In this work, we assume that the flux is given by generalized Fick's law

$$\mathbf{J}(\mathbf{r}, t) = - \sum_q D_q(K(\rho), \mathbf{r}, t) \nabla \nabla^{2q} \rho(\mathbf{r}, t), \quad (1)$$

where $D_q(K(\rho), \mathbf{r}, t)$ are diffusion coefficients depending in the Gaussian curvature K

of solvent density isosurfaces, and high order terms (i.e., $q > 1$) describe the influence of inhomogeneity in the solvent density and flux-flux correlation in the density flux. In particular, the term $\nabla\nabla^2$ can be regarded as an energy flux operator. A similar fourth order flux term was employed in the Cahn-Hilliard equation [3] to describe the evolution of a conserved concentration field during phase separation. The total solvent in the volume is given by $\int_{\Omega} \rho(\mathbf{r}, t) d\mathbf{r}$. The rate of change of the solvent in the volume, $\frac{d}{dt} \int_{\Omega} \rho(\mathbf{r}, t) d\mathbf{r}$, is balanced by the solvent out flux, $-\int_{\partial\Omega} \mathbf{J} \cdot \mathbf{n}(\mathbf{r}) dS$, and solvent production, $\int_{\Omega} P(K(\rho), \rho, \mathbf{r}, t) d\mathbf{r}$

$$\int_{\Omega} \frac{d}{dt} \rho(\mathbf{r}, t) d\mathbf{r} = - \int_{\partial\Omega} \mathbf{J} \cdot \mathbf{n}(\mathbf{r}) dS + \int_{\Omega} P(K(\rho), \rho, \mathbf{r}, t) d\mathbf{r} \quad (2)$$

where $\mathbf{n}(\mathbf{r})$ is the unit outer normal direction at \mathbf{r} . By using the divergence theorem, we convert the surface integral into a volume integral and obtain

$$\frac{\partial \rho(\mathbf{r}, t)}{\partial t} = \sum_q \nabla \cdot D_q(K(\rho), \mathbf{r}, t) \nabla \nabla^{2q} \rho(\mathbf{r}, t) + P(K(\rho), \rho, \mathbf{r}, t). \quad (3)$$

The diffusion coefficients $D_q(K(\rho), \mathbf{r}, t)$ are position dependent because of the possible presence of inhomogeneity, such multivalent ions [25], and their curvature-dependence is designed for the geometric control of solvent density isosurfaces in the final diffusion map. For example, the solvent density distribution near the molecular surface can be made to preserve the curvature of the probe molecule by taking $D_q(K(\rho), \mathbf{r}, t) \sim \exp\left(-\frac{(K-K_p)^2}{2\kappa_q^2}\right)$, where K_p is the Gaussian curvature of the probe and κ_q are constants. The solvent production can be either negative or positive, and is designed for further geometric control of the molecular surface. It can also be used to add or remove atoms at specific locations. High order gradient-controlled diffusion equations were proposed by Wei [31] for efficient image processing. Anisotropic reaction-diffusion equations have been introduced for shock-capturing in the context of computational fluid dynamics [32].

In this work, we define the problem of finding molecular multiresolution surfaces as an initial-boundary value problem governed by the new curvature-controlled diffusion equation (3) in a domain Ω that is large enough to include all the surfaces of interest of a molecule. The Dirichlet boundary condition is employed at domain boundary $\partial\Omega$, i.e., $\rho(\mathbf{r}, t) = \rho_0$, $\mathbf{r} \in \partial\Omega$. Initially, there is no presence of solvent in the domain, i.e., $\rho(\mathbf{r}, 0) = 0$, $\mathbf{r} \in \Omega$. We set $D_q(K(\rho), \mathbf{r}, t) = 0$ indiscriminately in all the atomic volumes $V_i = \frac{4}{3}\pi r_i^3$, where r_i is the i^{th} atom of the molecule. We choose the evolution time sufficiently long so that the solvent density can reach the center of the computational domain. The diffusion of the solvent toward to the domain center leads to a family of profiles of solvent density distribution, which in turn gives rise to a family of molecular multiresolution surfaces, corresponding to different solvent probe radii r_p and different resolutions. Note that the van der Waals surface, $\partial\Omega_{VWS}$, corresponds to $r_p = 0$, and is obtained at the level set $\rho = 0$. Here we define the midway molecular surface as the multiresolution molecular surface whose convex surfaces locate at the middle of

the van der Waals surface and the solvent accessible surface. Such a surface should be useful as it unclear whether the solvent accessible surface or the solvent excluded surface better describes hydration effects [16]. In general, the nonlinear terms in Eq. (3) can be utilized to provide large gradient near the desirable molecular surface. This approach directly results in a Cartesian grid representation of the molecular surface. Such a representation is important for many applications, particularly for implicit solvent modeling of electrostatics in macromolecules [26].

In general, it might not be convenient to solve the nonlinear reaction-diffusion equation (3). Thus simplifications are desirable. For homogeneous solvent, it is sufficient to set D_1 a piecewise constant $D_1 = D(\mathbf{r})$, and $D_q = 0$ if $q \neq 1$. For simplicity, we also drop the production term in the rest of discussion. Therefore, we arrive at a much simpler problem of diffusion

$$\begin{aligned} \frac{\partial \rho(\mathbf{r}, t)}{\partial t} &= \nabla \cdot D(\mathbf{r}) \nabla \rho(\mathbf{r}, t), \quad \mathbf{r} \in \Omega \\ \rho(\mathbf{r}, t) &= \rho_0, \quad \mathbf{r} \in \partial\Omega \\ \rho(\mathbf{r}, 0) &= 0, \quad \mathbf{r} \in \Omega \\ D(\mathbf{r}) &= 1, \quad \mathbf{r} \in \Omega/V_{WV}, \\ D(\mathbf{r}) &= 0, \quad \mathbf{r} \in V_{WV}, \end{aligned} \tag{4}$$

where V_{WV} is the molecular van der Waals volume given by $V_{WV} = \bigcup_i V_i$. However, the resulting diffusion equation does not yet admit a closed-form solution due to the irregular atomic surface information in $D(\mathbf{r})$. Fortunately, the numerical solution of Eq. (4) is quite robust. For example, both implicit and explicit approaches, as well as various spatial discretizations can be used to generate the solvent density profiles near the van der Waals surface.

The van der Waals surface generated by this approach is exact in the sense that its resolution is only limited by the finite mesh size. However, the molecular surface, or the solvent excluded surface computed in this manner could be distorted because the different diffusion path length for each different part of a molecular. To eliminate this error of molecular anisotropy, we set the computational boundary to be the solvent accessible surface ($\partial\Omega = \partial\Omega_{SAS}$). To this end, we define solvent-accessible radius of i^{th} atom as the sum of its atomic radius and the probe radius, $r_i^{SAR} = r_i + r_p$. The volume associated with solvent-accessible radius of the i^{th} atom is given by $V_i^{SAR} = \frac{4}{3}\pi [r_i^{SAR}]^3$. We initialize the solvent density on the desirable solvent accessible surface by setting $\rho(\mathbf{r}, 0) = 0, \quad \forall \mathbf{r} \in \bigcup_i V_i^{SAR}$ and $\rho(\mathbf{r}, 0) = \rho_0$ in rest of the domain. A large probe radius r_p can be chosen to ensure a variety of molecular multiresolution surfaces. Note that solvent accessible surface marked out by the solvent density $\rho(\mathbf{r}, 0)$ is also exact.

To speed up the solution of Eq. (4), we introduce a fast local spectral evolution kernel (LSEK) method [33], which is able to analytically solve a class of reaction-diffusion-convection equations $\frac{\partial}{\partial t} \rho = \left[D(t) \frac{\partial^2}{\partial x^2} + C(t) \frac{\partial}{\partial x} + P(t) \right] \rho$ in a single time step. The LSEK is exact in time and is of controllable accuracy in space. Its complexity at a fixed

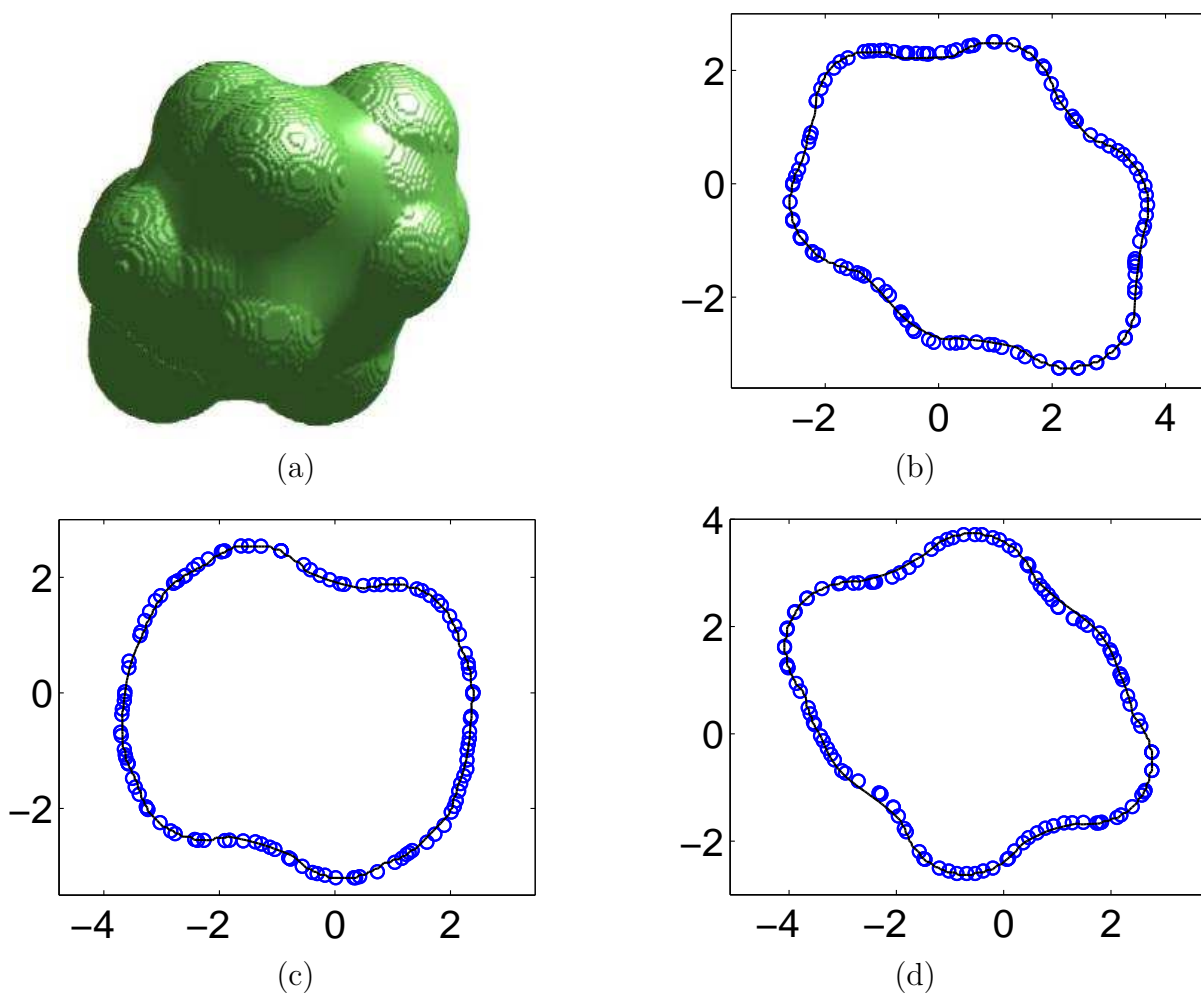


Figure 3: Molecular multiresolution surfaces of cyclohexane and their comparison with those obtained by the MSMS (Solid lines: present; Circles: MSMS). (a) The solvent excluded surface; (b) The cross section at $x = 0.6$; (c) The cross section at $y = 0.6$; (d) The cross section at $z = 0.6$.

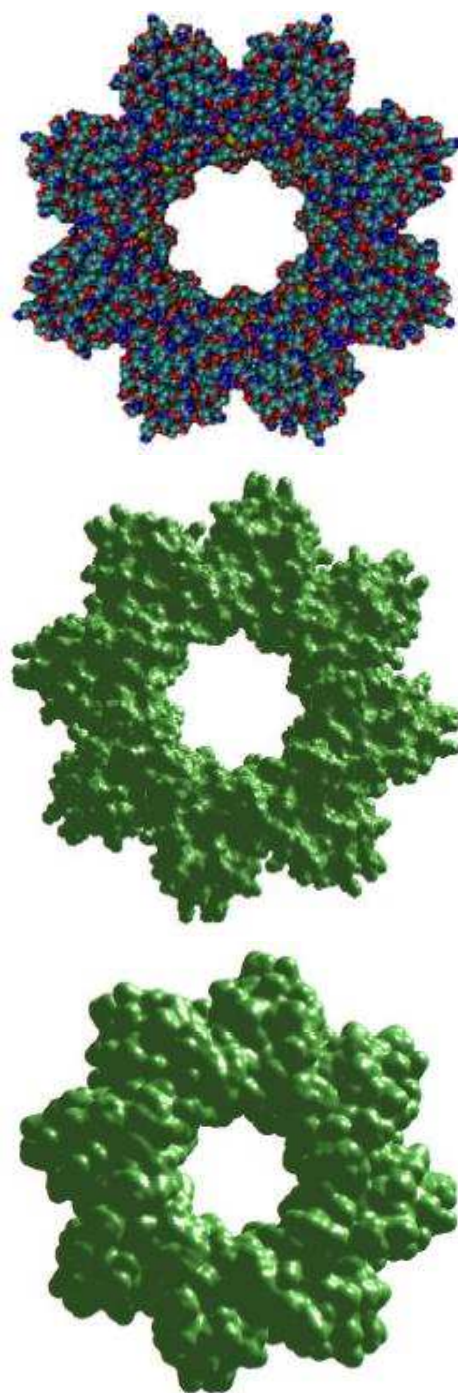


Figure 4: Molecular multiresolution surfaces of the cell division protein. Top: The van der Waals surfaces; Middle: The solvent excluded surface; Bottom: The midway molecular surface.

level of accuracy scales as $O(N)$, where N is the number of grid points. The solution of Eq. (4) at an arbitrary point of space-time, (x_i, y_j, z_k, t) , is obtained in a finite difference manner

$$\rho(x_i, y_j, z_k, t) = \sum_{l_x=-M_x}^{M_x} \sum_{l_y=-M_y}^{M_y} \sum_{l_z=-M_z}^{M_z} K_{h_x, \sigma_x}(l_x h_x, t) K_{h_y, \sigma_y}(l_y h_y, t) K_{h_z, \sigma_z}(l_z h_z, t) \rho(x_i - l_x h_x, y_j - l_y h_y, z_k - l_z h_z, 0), \quad (5)$$

where $2M_\alpha + 1$ are the stencil width for $\alpha = x, y, z$, h_α the grid spacings, and $K_{h, \sigma}(x, t)$ the LSEK [33]

$$K_{h, \sigma}(x, t) = \frac{h}{\sigma} \sum_{n=0}^{M_h/2} \left(-\frac{1}{4}\right)^n \frac{1}{\sqrt{2\pi}n!} \left(\frac{\sigma}{\sigma_t}\right)^{2n+1} h_{2n}\left(\frac{x}{\sqrt{2}\sigma_t}\right). \quad (6)$$

Here $h_{2n}(x)$ is the Hermite function defined by the Hermite polynomial H_{2n} , i.e., $h_{2n}(x) = \exp(-x^2)H_{2n}(x)$, M_h is the highest degree of Hermite polynomial used, σ is window parameter and $\sigma_t^2 = \sigma^2 + 2 \int_0^t D(s)ds$. We set $M_h = 88$, $M_\alpha = 32$ and $\sigma_\alpha = 3.05h_\alpha$ in this work.

As a proof of principle, we present two examples. In the first example, cyclohexane (C_6H_{12}), a test case recommended by Sanner *et al.* [27], is considered to validate the proposed method for calculating the solvent excluded surface. The van der Waals radii of the carbon and hydrogen atoms are taken as 1.7 and 1.2 Å, respectively. We choose a grid of 200 points in each dimension and set $\rho_0 = 100$, $r_p = 1.5$ Å. The solvent excluded surface is extracted at $\rho(\mathbf{r}, 12) = 0.04$, see Fig. 3a. We also compute the solvent excluded surface of cyclohexane by using the MSMS algorithm [27]. A comparison of three cross sections generated from the present approach and those from the MSMS is depicted in Figs. 3b-d. There is an excellent agreement among these results.

We next consider a cell division and cell wall biosynthesis protein [4]. It has 9772 atoms in eight polymer chains and 1328 residues. We choose the same set of computational parameters as those described in the preceding paragraph. Three multiresolution molecular surfaces, the van der Waals surface, the the solvent excluded surface, and the midway molecular surface of the cell division protein are depicted in Fig. 4. It is seen that the midway molecular surface captures the symmetry and other main features of the protein structure while avoids unnecessary details.

In summary, we have introduced a new concept, molecular multiresolution surfaces, for the multiscale modeling of biomolecules. The proposed concept provides a unified description of the van der Waals surface, solvent accessible surface and solvent excluded surface. A novel approach based on the controlled diffusion of continuum solvent density is proposed to generate the multiresolution surfaces. A fast local spectral evolution kernel is introduced to integrate the diffusion equation in a single time step. The proposed method does not need to discriminate buried atomic surfaces from unburied ones during the computation. It by passes the difficulty of singularities in other existing methods.

Numerical experiments are carried out to validate and demonstrate the proposed approach. The formulation and examples given here hopefully will spur the interest of other investigators in this and related fields.

References

- [1] N.A. Baker, D. Sept, M.J. Holst and J.A. McCammon, The adaptive multilevel finite element solution of the Poisson-Boltzmann equation on massively parallel computers, *IBM J. Res. Dev.*, **45**, 427-438 (2001).
- [2] C.A.S. Bergstrom, M. Strafford, L. Lazorova, A. Avdeef, K. Luthman and P. Artursson, Absorption classification of oral drugs based on molecular surface properties, *J. Medicinal Chem.*, **46**, 558-570 (2003).
- [3] J.W. Cahn and J.E. Hilliard, Free energy of nonuniform system. I. Interfacial free energy, *J. Chem. Phys.*, **28**, 258-267 (1958).
- [4] S. Chen, J. Jancrick, H. Yokota, R. Kim and S.-H. Kim, Crystal structure of a protein associated with cell division from *Mycoplasma pneumoniae* (GI: 13508053): a novel fold with a conserved sequence motif, *Proteins*, **55**, 785-791 (2004).
- [5] M.L. Connolly, Analytical molecular surface calculation, *J. Appl. Crystallogr.*, **16**, 548-558 (1983).
- [6] M.L. Connolly, Molecular surface triangulation, *J. Appl. Crystallogr.*, **18**, 499-505 (1985).
- [7] P.B. Crowley and A. Golovin, Cation-pi interactions in protein-protein interfaces, *Proteins - Struct. Func. Bioinf.*, **59**, 231-239 (2005).
- [8] B. Das and H. Meirovitch, Optimization of solvation models for predicting the structure of surface loops in proteins, *Proteins*, **43**, 303-314 (2001).
- [9] A.I. Dragan, C.M. Read, E.N. Makeyeva, E.I. Milgotina, M.E.A. Churchill, C. Crane-Robinson and P.L. Privalov, DNA binding and bending by HMG boxes: Energetic determinants of specificity, *J. Mol. Biol.*, **343**, 371-393 (2004).
- [10] F. Eisenhaber and P. Argos, Improved strategy in analytic surface calculation for molecular systems: Handling of singularities and computational efficiency, *J. Comput. Chem.*, **14**, 1272-1280 (1993).
- [11] M.S. Lee, M. Feig, F.R. Salsbury and C.L. Brooks, New analytic approximation to the standard molecular volume definition and its application to generalized born calculations, *J. Comput. Chem.*, **24**, 1348-1356 (2003).

- [12] R. Fraczekiewicz and W. Braun, Exact and efficient analytical calculation of the accessible surface areas and their gradients for macromolecules, *J. Comput. Chem.*, **19**, 319-333 (1998).
- [13] K.D. Gibson and H.A. Scheraga, Exact calculation of the volume and surface area of fused hard-sphere molecules with unequal atomic radii, *Mol. Phys.*, **62**, 1247-1265 (1987).
- [14] V. Gogonea and E. Osawa, Implementation of Solvent Effect in Molecular Mechanics. 1. Model Development and Analytical Algorithm for the Solvent -Accessible Surface Area, *Supramol. Chem.*, **3**, 303-317 (1994).
- [15] J. Greer and B. Bush, Macromolecular shape and surface maps by solvent exclusion, *Proc. Natl. Acad. Sci. USA*, **75**, 303-307 (1978).
- [16] R.M. Jackson and M.J. Sternberg, A continuum model for protein-protein interactions: application to the docking problem , *J. Mol. Biol.*, **250**, 258-275 (1995).
- [17] B. Lee and F.M. Richards, Interpretation of protein structures: estimation of static accessibility , *J. Mol. Biol.*, **55**, 379-400 (1973).
- [18] J. Liang, H. Edelsbrunner, P. Fu, P.V. Sudhakar and S. Subramaniam, An analytical shape computation of macromolecules: I. molecular area and volume through alpha shape, *Proteins*, **33**, 1-17 (1998).
- [19] V.J. LiCata and N.M. Allewell, Functionally linked hydration changes in Escherichia coli aspartate transcarbamylase and its catalytic subunit, *Biochemistry*, **36**, 10161-10167 (1997).
- [20] J.R. Livingstone, R.S. Spolar and M.T. Jr. Record, Contribution to the thermodynamics of protein folding from the reduction in water-accessible nonpolar surface area, *Biochemistry*, **30**, 4237-4244 (1991).
- [21] B. Mandelbrot, How long is the coast of Great Britain - Statistical self-similarity and fractional dimension, *Science*, **155**, 636-638 (1967).
- [22] T.M. Raschke, J. Tsai and M. Levitt, Quantification of the hydrophobic interaction by simulations of the aggregation of small hydrophobic solutes in water, *Proc. Natl. Acad. Sci. USA*, **98**, 5965-5969 (2001).
- [23] F.M. Richards, Areas, volumes, packing and protein structure, *Annu. Rev. Biophys. Bioeng.*, **6**, 151-176 (1977).
- [24] T.J. Richmond, Solvent accessible surface area and excluded volume in proteins. Analytical equations for overlapping spheres and implications for the hydrophobic effect , *J. Mol. Biol.*, **178**, 63-89 (1984).

- [25] W. Rocchia, E. Alexov and B. Honig, Extending the applicability of the nonlinear Poisson-Boltzmann equation: Multiple dielectric constants and multivalent ions, *J. Phys. Chem. B*, **105**, 6507-6514 (2001).
- [26] W. Rocchia, S. Sridharan, A. Nicholls, E. Alexov, A. Chiabrera and B. Honig, Rapid grid-based construction of the molecular surface and the use of induced surface charge to calculate reaction field energies: Applications to the molecular systems and geometric objects, *J. Comput. Chem.*, **23**, 128-137 (2002).
- [27] M.F. Sanner, A.J. Olson and J.C. Spohner, Reduced surface: An efficient way to compute molecular surfaces, *Biopolymers*, **38**, 305-320 (1996).
- [28] R.S. Spolar and M.T. Jr. Record, Coupling of local folding to site-specific binding of proteins to DNA, *Science*, **263**, 777-184 (1994).
- [29] M. Totrov and R. Abagyan, The contour-buildup algorithm to calculate the analytical molecular surface, *J. Struct. Biol.*, **116**, 138-143 (1996).
- [30] A. Varshney and F. P. Jr. Brooks and W. V. Wright, Computing smooth molecular surfaces, *IEEE Comp. Graph. Appl.*, **14**, 19-25 (1994).
- [31] G. W. Wei, Generalized Perona-Malik equation for image restoration, *IEEE Sig. Proc. Lett.*, **6**, 165-167 (1999).
- [32] G.W. Wei, Oscillation reduction by anisotropic diffusions, *Comput. Phys. Commun.*, **144**, 417-342 (2002).
- [33] S.N. Yu, S. Zhao and G.W. Wei, Local spectral time splitting method for first and second order partial differential equations, *J. Comput. Phys.*, **206**, 727-780 (2005).
- [34] R.J. Zauhar and R.S. Morgan, Computing the electric-potential of biomolecules - application of a new method of molecular-surface triangulation, *J. Comput. Chem.*, **11**, 603-622 (1990).